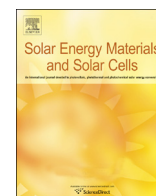




ELSEVIER

Contents lists available at ScienceDirect

Solar Energy Materials & Solar Cells

journal homepage: www.elsevier.com/locate/solmat

Indium-free multilayer semi-transparent electrodes for polymer solar cells

Alexander T. Barrows^a, Rob Masters^b, Andrew J. Pearson^{a,1}, Cornelia Rodenburg^b, David G. Lidzey^{a,*}^a Department of Physics and Astronomy, The University of Sheffield, Hicks Building, Hounsfield Road, Sheffield S3 7RH, UK^b Department of Materials Science and Engineering, The University of Sheffield, Sir Robert Hadfield Building, Mappin Street, Sheffield S1 3JD, UK

ARTICLE INFO

Article history:

Received 20 July 2015

Received in revised form

8 October 2015

Accepted 11 October 2015

Keywords:

Organic solar cell

Transparent electrode

ITO free electrode

ABSTRACT

We have explored the fabrication of indium-free electrodes for use in a PCDTBT:PC₇₀BM organic photovoltaic (OPV) device, and compare different multilayer electrodes as the device anode. Two oxide/metal/oxide structures were investigated that consisted of MoO₃/Ag/MoO₃ (MAM) and TeO₂/Ag/MoO₃ (TAM) multilayers. Using scanning electron microscopy measurements, we find that the electrode utilising a TeO₂ seed layer encouraged the growth of a more continuous silver layer at low film thickness relative to an MoO₃ seed layer, and thus combines enhanced optical transmission (by around 7%) with low sheet resistance (14 Ω/□). This enhanced optical transmittance results in an increased short-circuit current in photovoltaic cells, with TAM-based devices having a power conversion efficiency around 6% higher than those fabricated using a comparable MAM electrode.

© 2015 Elsevier B.V.. Published by Elsevier B.V. This is an open access article under the CC BY license (<http://creativecommons.org/licenses/by/4.0/>).

1. Introduction

In the decade to the end of 2014, world primary-energy consumption grew on average by 2.1% per year [1]. Against this background there is increasing concern about climate change, resource constraints and the security of energy supply, leading to great interest in renewable energy generation. Photovoltaics are expected to play a major role in this sector, and whilst silicon currently dominates the market [2], organic photovoltaics (OPVs) are a promising route to lowering the cost of solar power. The solution processed nature of the photoactive layer allows for the possibility of high throughput production via roll-to-roll techniques such as spray coating or printing [3,4], and in addition OPVs can be fabricated on flexible, lightweight substrates such as PET [5–7] or even metal foils [8,9].

Due to its combination of high transmittance and good conductivity, indium tin oxide (ITO) is currently the ubiquitous material used as the transparent front electrode in OPVs. There are, however, concerns about the cost and scarcity of indium [7,10] and the embodied energy of the ITO layer [11,12]. Furthermore, high quality ITO is not easily compatible with the cheap, flexible

polymer substrates that facilitate roll-to-roll production processes, as the brittle-nature of ITO results in a significant increase in sheet resistance after repeated bending [13,14]. Furthermore, such polymer substrates cannot tolerate the high temperatures that are commonly used in the deposition of highly conductive ITO. This second limitation leads to the sheet resistance of ITO on PET being around five times higher than that of similar ITO layers on glass [5,15–17].

There has thus been significant interest in the development of alternative materials for use as transparent conductive electrodes in OPVs. Here, possible replacements include the highly conductive polymer PEDOT:PSS in combination with metal grids [18,19], carbon nanosheets [20], silver nanowires [21–23] and oxide/metal/oxide stacks. In such oxide/metal/oxide multilayer electrodes, the initial oxide layer acts as a ‘seed layer’ for the subsequent growth of an ultrathin metal film. When used in an OPV, the metal film provides high lateral conductivity ensuring a suitably low series resistance, with the second oxide layer facilitating charge extraction or charge-blocking from the device [24,25]. In addition to their electronic functionality, such oxide layers also suppress reflection from the metal film and maximise optical transmittance [26–29].

In this paper, we explore two different oxide/metal/oxide stacks as the hole extracting electrode in an OPV device based on the polymer:fullerene blend PCDTBT:PC₇₀BM. Whilst MoO₃/Ag/MoO₃ (MAM) electrodes have previously been investigated for use

* Corresponding author.

E-mail address: d.g.lidzey@sheffield.ac.uk (D.G. Lidzey).¹ Present address: Cavendish Laboratory, JJ Thomson Avenue, Cambridge CB3 0HE, UK.

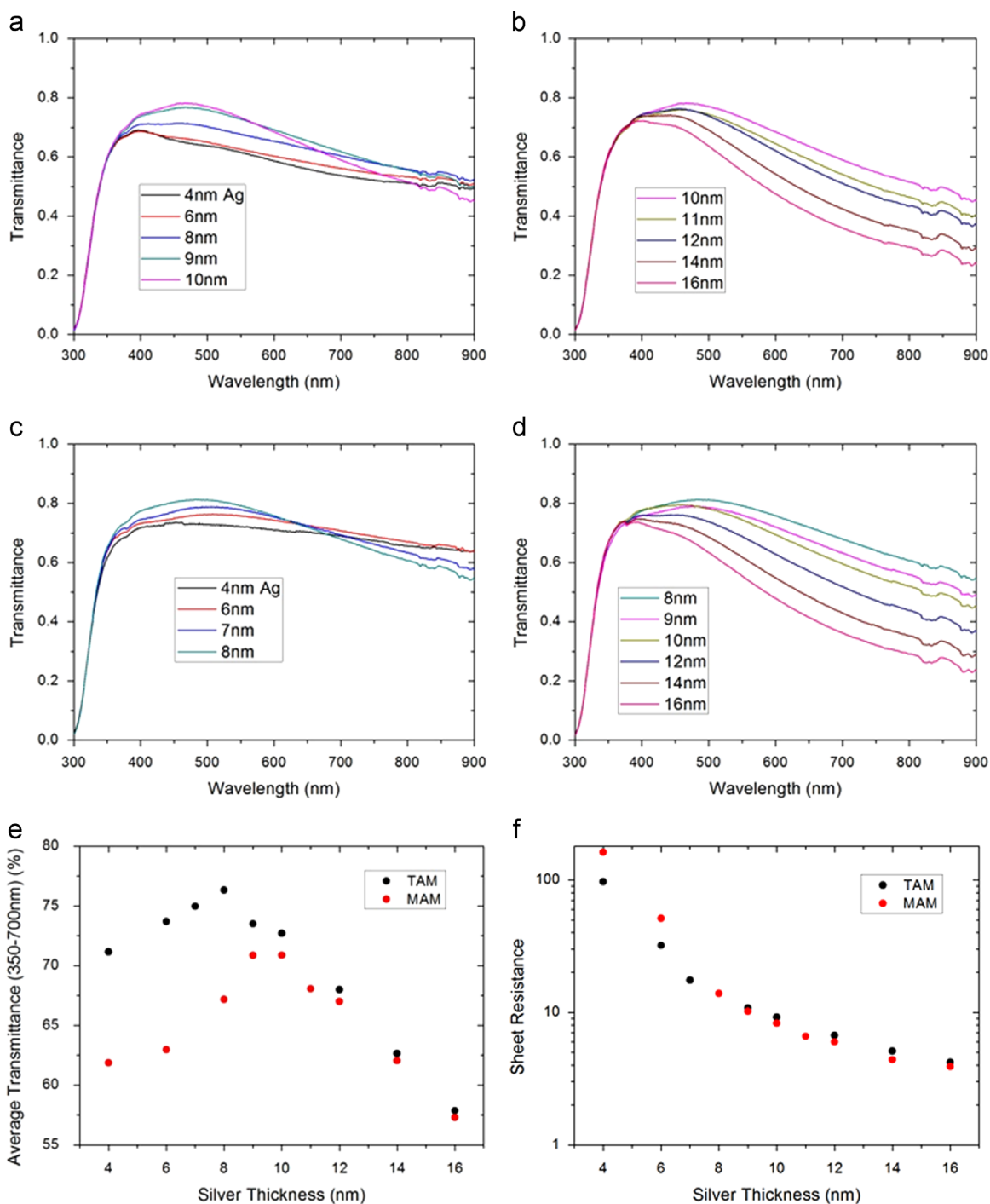


Fig. 1. Transmittance spectra for multilayer MAM ((a) and (b)) and TAM ((c) and (d)) electrodes on glass with varying thickness of the silver film. All spectra are referenced to air, meaning that the spectra presented herein include reflection and absorption by the glass substrate. Average transmittance in the 350–700 nm range (e) and sheet resistance (f) for varying silver thicknesses are also shown. In all cases the oxide layers are all kept at a thickness of 10 nm.

in OPVs [30–33], $\text{TeO}_2/\text{Ag}/\text{MoO}_3$ (TAM) electrodes have not. One study which investigated a $\text{TeO}_2/\text{Ag}/\text{PEDOT:PSS}$ electrode [34] suggested that a tellurium dioxide seed layer should lead to an enhanced short circuit current (J_{SC}) in comparison with an equivalent $\text{MoO}_3/\text{Ag}/\text{PEDOT:PSS}$ structure, resulting from the larger (real-part) refractive index of TeO_2 [27]. Whilst the devices fabricated using such electrodes achieved a promising performance, the expected enhancement in J_{SC} resulting from the use of TeO_2 was not verified experimentally. Here we find that replacement of the MoO_3 seed layer by TeO_2 leads to significantly higher transmittance at low silver thickness, attributable to the formation

of a more continuous silver layer, as observed by scanning electron microscopy (SEM). When applied as the window electrode in PCDTBT:PC₇₀BM polymer solar cells the improved transmittance of the TAM electrode results in an increased J_{SC} in comparison to devices based on a MAM electrode.

2. Experimental

The TAM and MAM devices explored were deposited upon 1.1 mm thick quartz-glass substrates. As a control, identical devices

consisting of a MoO₃ hole-extraction layer deposited on an ITO electrode were also fabricated. Both quartz-glass substrates and pre-patterned ITO films were purchased from Ossila Limited. To prepare the quartz-substrates, they were initially cleaned by sequential sonication in warm Helmanex solution, IPA and deionised water for 5 min before being dried with compressed nitrogen and transferred to a nitrogen glovebox connected to a thermal evaporator. All subsequent thin-film evaporations were performed at a base pressure of $<5 \times 10^{-6}$ mbar through a shadow mask. Evaporation of molybdenum oxide pellets (99.95%, Testbourne), tellurium dioxide powder (99.995% trace metals basis, Sigma-Aldrich) and silver shot ($\geq 99.99\%$ trace metals basis, Sigma-Aldrich) were performed at rates of 0.3, 0.3 and 5.0 Ås⁻¹ respectively. Transmittance spectra were measured using a Horiba FluoroMax-4 and are referenced to air. Sheet resistance was measured using a 4 point probe. SEM images were recorded using an FEI Nova NanoSEM 450 scanning electron microscope. A solid-state backscatter detector was used with a 3 kV primary beam, 5 mm working distance and a -4 kV beam deceleration field applied. Atomic force microscopy measurements were obtained using a Veeco Dimension 3100 with tips from Budget Sensors (300G-Al). Data analysis was performed using the Gwyddion software package.

The active layer of the OPV device was based on a blend of the polymer PCDTBT with the fullerene acceptor PC₇₀BM. The PCDTBT solution was prepared by adding the dry polymer to chlorobenzene, after which it was stirred at 70 °C for 24 h before being added to PC₇₀BM to produce a 1:4 blend of PCDTBT:PC₇₀BM at a concentration of 20 mg/ml. The solution was then heated to 70 °C and stirred for a further 24 h to fully solubilise both materials. This solution was cooled to room-temperature, filtered with a 0.45 µm PTFE filter and spin-coated onto the anode at a spin speed between 600 and 2000 rpm, producing a layer having a thickness between 50 and 105 nm (as measured using a Dektak surface profilometer). A top cathode layer was then deposited onto the active layer by a sequential thermal evaporation of 6.5 nm calcium followed by 100 nm aluminium. In all cases, devices thus had a layer structure of glass/anode/PCDTBT:PC₇₀BM/Ca/Al. Finished devices were encapsulated using a glass slide and a UV epoxy (Ossila Ltd.) that was cured under a UV lamp for 30 min before being removed from the glovebox for testing. OPV devices were tested using a Newport 92251A-1000 solar simulator (AM1.5 spectrum at an intensity of 1000 W/m²) through a 0.025 cm² aperture mask used to define the illuminated area. The data presented represents an average over 16 devices from 4 separate substrates for each type of anode tested. We only report the efficiency of the best 50% of devices, thus excluding pixels containing a significant defect, whilst avoiding the use of a statistical method that is open to user bias.

The optical properties of electrodes and OPV devices were modelled using a freely available program based on the transfer matrix method [35]. The optical constants for ITO, Ag, Al and Ca were taken from the library associated with this model, whilst those for MoO₃, TeO₂ and the photoactive blend were determined using an M2000v J.A. Woollam Co. spectroscopic ellipsometer.

3. Results and discussion

3.1. Optical and electrical properties of TeO₂ and MoO₃ based electrodes

To explore the effect of the structure of the oxide/metal/oxide multilayers on their optical properties, we fabricated a series of structures in which the thickness of the metal (silver) film was varied. The thickness of all films was determined by the film thickness monitor in the evaporation chamber. Note that such

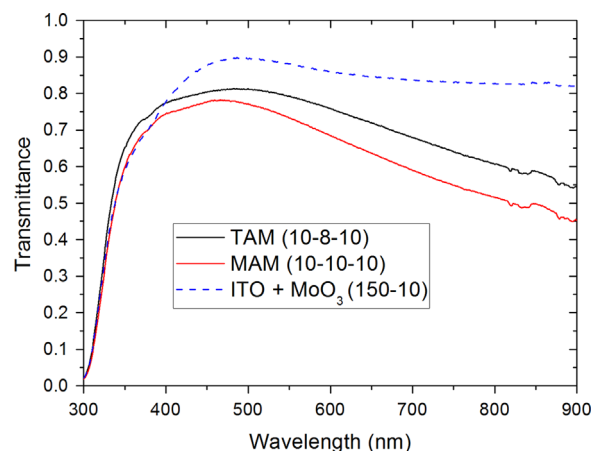


Fig. 2. Transmittance spectra for the TAM and MAM multilayer electrodes with layer thicknesses of 10–8–10 nm and 10–10–10 nm respectively (i.e. with silver layer thickness corresponding to the percolation threshold for that structure). The spectrum for the ITO/MoO₃ anode used on reference devices is also presented.

thicknesses should be considered as an average value, as the films are highly structured at nanometre length-scales (*vide infra*). In Fig. 1(a) and (b) we plot transmittance spectra for multilayer MAM electrodes as the silver-film thickness was varied between 4 and 10 nm (part (a)) and 10 and 16 nm (part (b)). In Fig. 1(c) and (d), we similarly show transmittance spectra for the TAM electrodes as the thickness of the silver was varied between 4 and 8 nm (part (c)) and 8 and 16 nm (part (d)). In all cases, the thickness of the oxide films (both MoO₃ and TeO₂) was fixed at 10 nm. In line with other reports on oxide/metal/oxide structures, we find that (counter-intuitively) the transmittance of the film initially increases with increasing thickness of the silver layer, before reaching a maximum at a thickness termed the percolation threshold. Above this thickness, the transmittance of the multilayer reduces, an effect particularly pronounced at longer wavelengths as a result of the silver film acting as a mirror. It can be seen that for our MAM electrodes the maximum transmittance occurs at a silver thickness of 10 nm; a result comparable to other literature values for the percolation threshold of Ag on MoO₃ (being between 10 and 11 nm [30–32]). For the TAM electrodes, the maximum transmittance occurs at a reduced silver thickness of 8 nm. We summarise the average transmittance of the MAM and TAM electrodes over the wavelength-range 350–700 nm in Fig. 1(e), where it can be seen that over the Ag thickness range 4–8 nm average transmittance rises from 62–67% for the MAM structure and 71–76% for the TAM structure.

We have also measured the sheet resistance of the films as a function of the thickness of the silver layer, with data presented in Fig. 1f. It can be seen that for both the MAM and TAM electrodes there is a rapid decrease in sheet resistance as the thickness of the silver layer increases, however this decrease saturates as the film thickness exceeds the percolation threshold.

In Fig. 2, we illustrate the potential benefits of the use of the TAM structure as a transparent front electrode in an OPV, by plotting the relative transmission of the MAM and TAM electrodes at their percolation threshold (point of maximum optical transmittance). We find that the TAM electrode having an 8 nm thick silver layer has a maximum transmittance of 81.3%, an average transmittance (between 350 and 700 nm) of 76.3% and a sheet resistance of 13.9 Ω/□. In contrast a MAM electrode having a 10 nm thick silver layer has reduced maximum transmittance of 78.2% and an average transmittance (350–700 nm) of only 70.9%, with the sheet resistance being slightly lower at 8.3 Ω/□. For comparison, the reference ITO electrode (150 nm) coated with a 10 nm thick MoO₃ layer has a maximum transmittance of 89.8%, an

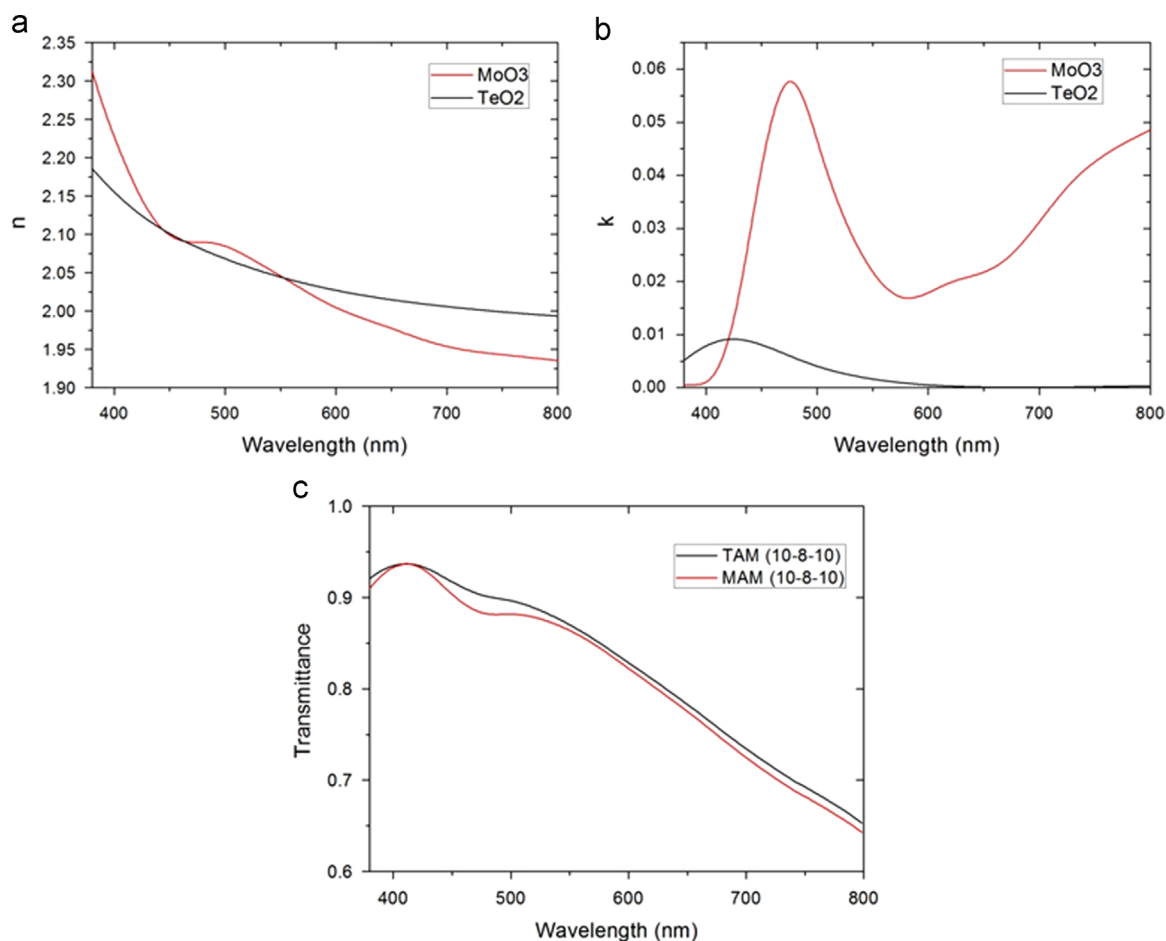


Fig. 3. (a) and (b) show the optical constants for thin MoO₃ and TeO₂ layers, as determined by ellipsometry. Modelled transmittance spectra for MoO₃/Ag/MoO₃ (MAM) and TeO₂/Ag/MoO₃ (TAM) multilayer electrodes with layer thickness of 10–8–10 nm are shown in (c).

average transmittance (350–700 nm) of 83.8% and a sheet resistance of $15.9 \Omega/\square$. Figs. 1e and f clearly show that for low thickness of the silver film, the TAM electrode has a significantly higher transmittance and somewhat lower sheet resistance than the corresponding MAM electrode. As the thickness of the silver increases, the relative improvement in transmittance afforded by the use of a TAM structure is reduced, with the transmission of the TAM electrode being only slightly greater than that of the MAM electrode at and above the percolation threshold. Above an Ag thickness of 8 nm, the sheet resistances of the TAM and MAM electrodes are similar.

3.2. Origin of enhanced transmittance in TeO₂ based electrodes

The trends observed in transmittance and sheet resistance as the silver layer thickness increases result from the growth characteristics of the metal film. As silver is deposited, it initially forms isolated islands and chains (so-called Volmer–Weber growth), resulting in poor lateral conductivity due to a lack of continuous conduction pathways. As the film thickness increases, the silver particles coalesce to form an increasingly uniform and continuous layer. The formation of continuous conduction pathways then results in a rapid reduction in sheet resistance, a process that slows once a uniform and well-connected film has been created. Whilst a number of studies have observed these same trends for a variety of oxide/metal/oxide structures, there is some disagreement as to the exact source of the initial increase in transmittance as the layer is deposited. Some studies attribute it simply to light scattering by the unconnected islands, with this scattering effect

being reduced as the layer becomes more uniform [36–38]. Others attribute it to surface plasmon resonance at the optimum thickness, with excitation of the surface plasmon only being achieved effectively for the structure which obtains maximum transmittance (due to the different sizes and spacing of metallic chains in films with different thickness) [39–41]. One recent study observed that as the film thickness increased, the film structure changed from one characterised by narrow cracks between metal islands and chains (usually unconnected) to a continuous structure with a random collection of nanoholes. It was proposed that the nanoholes allow for the formation of surface plasmon polaritons which propagate through the holes, with light then being re-radiated, thus increasing transmission. At higher thicknesses, such nanoholes become covered by the silver layer, and transmittance again drops [42].

We propose that our results can be explained by the formation of a more continuous silver layer at low thickness on a tellurium dioxide seed layer in comparison to silver films grown on a molybdenum oxide seed layer. The formation of a more continuous Ag layer on TeO₂ is consistent with the observed improvement in transmittance due to reduced scatter from unconnected islands, whilst the reduced sheet resistance at low silver thickness is similarly explained by the more continuous silver film. Overall, this effect allows the optimised TAM electrode to have a notably higher transmittance than can be obtained using a MAM electrode. This proposal is also consistent with the percolation threshold being reached at a comparatively reduced silver thickness on the TeO₂ seed layer compared to that observed on the MoO₃ seed layer (8 nm and 10 nm respectively). Clearly for Ag

thicknesses above the percolation threshold for both types of electrode, the silver films formed are quasi-continuous and no large differences in transmittance are observed. The formation of a more continuous silver film on TeO_2 is commensurate with previous work in which liquid Ag was found to have a slightly lower contact angle on TeO_2 than on MoO_3 [43]. This is indicative of stronger interactions between the silver and the TeO_2 , which will increase the energetic favourability of silver atoms becoming positioned on the metal oxide layer rather than aggregating into disconnected clusters. A lower contact angle will thus assist in the formation of a more continuous silver layer by encouraging growth to occur in a layer-by-layer manner (Frank–van der Merwe

growth) and reducing the favourability of island formation. The lower contact angle on a TeO_2 seed layer can be thought of as showing the improved wettability of liquid Ag on TeO_2 , which enhances the uniformity of the silver film. We note that modification of the seed layer to achieve a higher surface energy (giving stronger substrate–silver interactions) has previously been found to lead to the formation of a more continuous silver film in MAM electrodes [44].

We have modelled the optical properties of the multilayer stacks using a Transfer-Matrix model to explore whether differences in the refractive index (real and imaginary) of the seed layers play a significant role in modifying the optical transmission of the electrodes

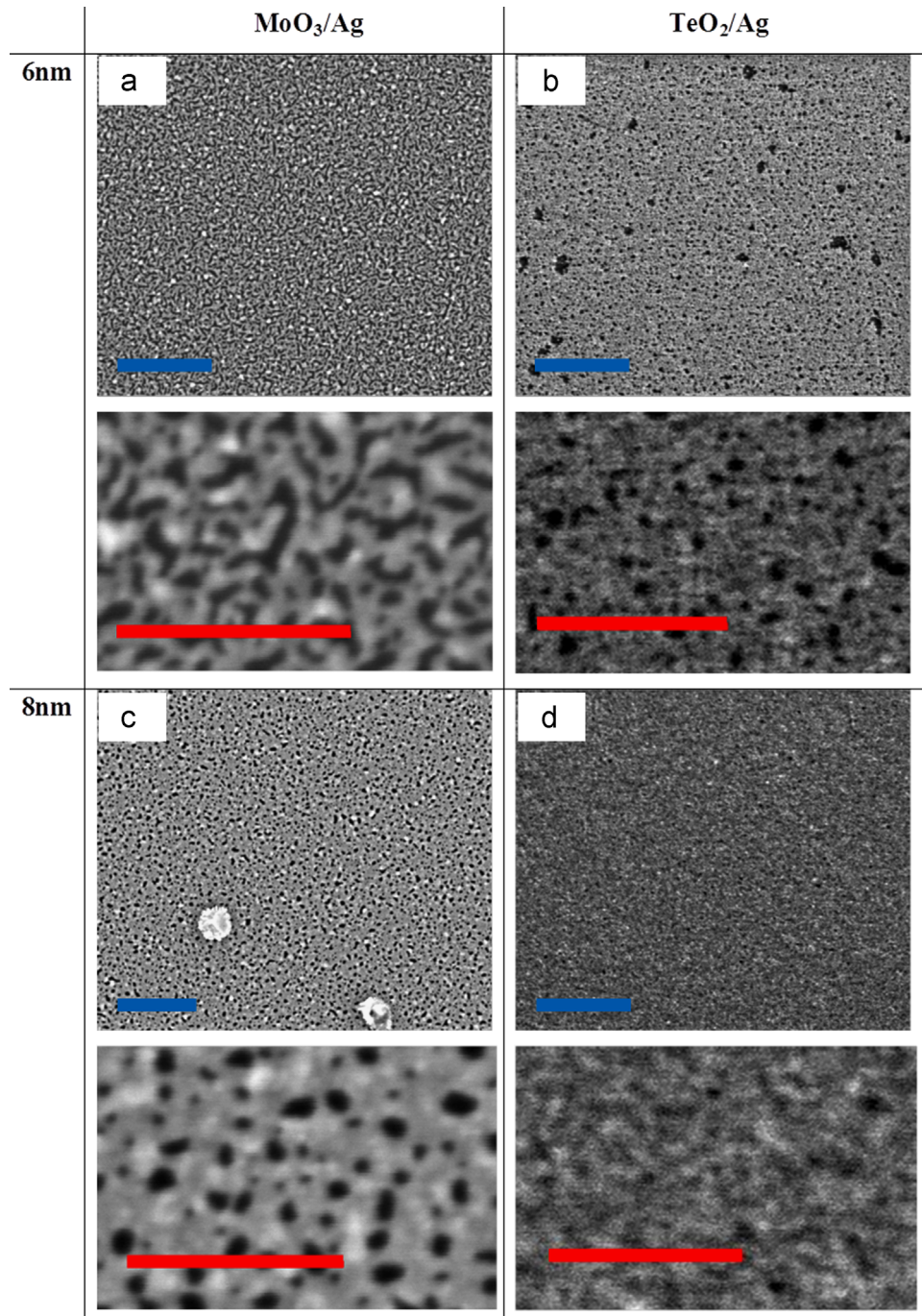


Fig. 4. SEM images of MoO_3/Ag and TeO_2/Ag bilayers in which the oxide thickness is fixed at 10 nm. Parts (a) and (c) show MoO_3/Ag bilayer for a silver thickness 6 nm and 8 nm respectively. Parts (b) and (d) similarly show a TeO_2/Ag bilayer again utilising a silver layer having a thickness of 6 nm and 8 nm respectively. Blue scale bars correspond to 500 nm. In each case, we show a magnified image of the film surface in which the length of the (red) scale bar is set at 200 nm.

[35]. The model assumes that all layers are uniform and continuous, and thus does not take into account the reduction in transmittance which occurs at silver film thickness below the percolation threshold for an oxide/metal/oxide structure. As input into this model, we have established n and k for TeO_2 and MoO_3 using spectroscopic ellipsometry as shown in Fig. 3(a) and (b) respectively. The calculated transmittance of MAM and TAM multilayer electrodes, (both having layer thickness of 10–8–10 nm) are shown in Fig. 3(c). It can be seen that our model suggests that over the wavelength region 380–800 nm, the MAM and TAM electrodes have an average transmittance of 81.2% and 82.1% respectively. The small enhancement in transmittance predicted for the TAM electrode results from the lower extinction coefficient of TeO_2 compared to MoO_3 , as well as its favourable refractive index (higher at longer wavelengths, lower at shorter wavelengths – see Fig. 3(a)). This result strongly suggests that the enhancements in transmittance in the TAM structures observed for silver thickness less than 10 nm can be attributed to the formation of a more continuous silver film rather than any optical effects resulting from the differing seed layer materials themselves, with the slightly increased transmission for the TAM structures compared to the MAM structures for thicker Ag films attributable to the favourable optical properties of TeO_2 .

To further explore the origin of the improved transmittance of the TAM electrodes at low Ag thickness, we have recorded SEM images of bilayer structures consisting of the metal oxide seed layer and an Ag layer. This is shown in Fig. 4, where we plot images for Ag films having a thickness of 6 nm and 8 nm on 10 nm thick seed layers of TeO_2 and MoO_3 . It can be seen that the 6 nm thick silver film deposited on MoO_3 (part (a)) is characterised by a series of thin “chains” having a typical width in the range 10–30 nm. Such structures presumably result in a non-continuous pathway for charge-carrier extraction. In contrast, the 6 nm thick silver film deposited on TeO_2 (part (b)) appears to be more continuous in nature and consists of a series of holes having a diameter of around 5–20 nm. Importantly, such films contain fewer isolated (unconnected) features. When the silver thickness is increased to 8 nm, the film on MoO_3 (part (c)) appears to have formed a more connected structure, whilst the film on TeO_2 (part (d)) exhibits fewer holes than with the 6 nm thick film. In fact, when we compare the magnified images of an 8 nm Ag film on MoO_3 (part (c)) with a 6 nm Ag film on TeO_2 (part (b)) we find that they appear qualitatively similar. This finding is commensurate with our measurements of their optical properties, in which we found that the percolation threshold occurred for Ag films that were 2 nm thinner on a TeO_2 seed layer compared to those on MoO_3 . Estimates of the coverage of the silver films from these SEM images also fit with this conclusion (see Table S2).

3.3. Indium-free polymer solar cells

In order to demonstrate the practical use of such electrodes, we have fabricated bulk heterojunction polymer solar cells based on a PCDTBT:PC₇₀BM photoactive layer using MAM, TAM and ITO/MoO₃ anodes. In each case, multilayer electrodes having the maximum transmittance were used; the MAM electrode thus utilised a 10 nm Ag layer whilst the TAM electrode incorporated a slightly thinner 8 nm Ag layer.

Again, we have used Transfer Matrix modelling to predict the optimum thickness of both the oxide layers in the multilayer electrode and the thickness of the PCDTBT:PC₇₀BM active-layer [35]. The model allows us to predict the short-circuit current of a device by assuming an internal quantum efficiency of 100% (i.e. ignoring possible charge extraction losses). We term this photocurrent as $J_{\text{SC},100\%}$. In our model, we adjust the thickness of the hole-extraction layer (the metal oxide layer placed adjacent to the

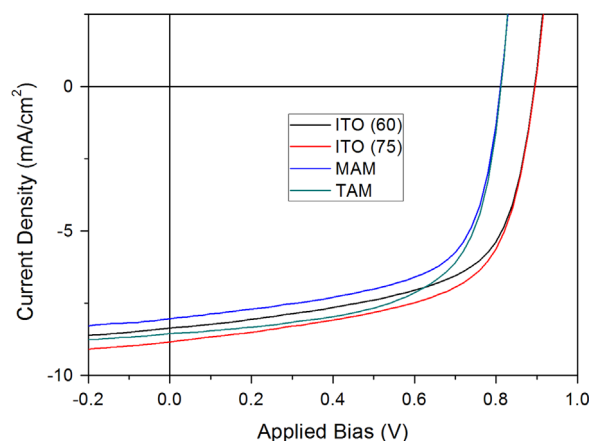


Fig. 5. Current-density against voltage curves for devices fabricated using the different anodes.

active layer), the thickness of the seed layer positioned beneath the Ag and the thickness of the active semiconductor layer. We find that for seed layers having a thickness ≥ 30 nm, our model predicts that $J_{\text{SC},100\%}$ is maximised, however this photocurrent is only marginally larger than that predicted when using a 5 nm seed layer. In fact, we find that by adjusting the thickness of the active layer, the $J_{\text{SC},100\%}$ takes values between 11.50 and 11.59 mA/cm² as the seed layer thickness varies from 5 to 40 nm. We note, however, that thicker seed layers require the use of slightly thicker active layers (by around 10 nm) in order to maximise $J_{\text{SC},100\%}$. Experimentally, increasing the thickness of the active layer is known to increase loss within the device as a result of increased non-geminate charge recombination. In addition, we found that a thinner seed layer lead to a slight reduction in sheet resistance and a better correspondence to the modelled transmittance (see Figure S1 and Table S1). For this reason, we used a relatively thin (5 nm) seed layer for the MAM and TAM electrodes – an approach that has also been used in other studies [45]. With this seed layer thickness of 5 nm we find that the average transmittance in the 350–700 nm range rises slightly from 70.9% to 71.7% for the optimised MAM electrode and from 76.3% to 77.1% for the optimised TAM electrode. Our model predicted that for both of these electrodes the optimum value of $J_{\text{SC},100\%}$ would occur for a metal oxide HTL having a thickness of 10 nm with the active layer having a thickness of 70 nm. Experimentally, however, we found that the optimum device efficiency occurred when the active-layer was slightly thinner (60 nm) than predicted by the model for both types of multilayer electrode. For devices utilising an ITO/MoO₃ electrode, our model similarly predicted an optimum active layer thickness of 85 nm, however experimental measurements determined the highest device efficiency was realised for an active layer thickness 75 nm (see Tables S3, S4 and S5 for details). In both cases, the discrepancy between the results of the model and the experimental device optimisation likely results from imperfect charge extraction through the active layer; an effect not considered by the model.

We tabulate average device parameters for solar cells fabricated using the three different types of anodes in Table 1. We find that the optimised devices using a TAM electrode had an average PCE of $(4.22 \pm 0.08)\%$ whilst the optimised MAM-electrode devices had a slightly lower average PCE of $(3.94 \pm 0.12)\%$. The improvement in efficiency for devices incorporating the TAM electrode results from a relative enhancement in J_{SC} by 7% (8.70 ± 0.12) mA/cm² compared with (8.11 ± 0.14) A/cm²; an effect that we attribute to the higher transmittance of the TAM electrode. The optimised ITO/MoO₃ reference device had the highest average PCE of $(4.81 \pm 0.09)\%$, again resulting from an enhanced J_{SC} of (9.12 ± 0.24) mA/cm². It is

Table 1
Electrode properties and solar cell performance for MAM (5–10–10), TAM (5–8–10) and ITO/MoO₃ (150–10) electrodes. The ITO electrode was tested with active layer thickness of both 60 nm and 75 nm. Standard deviations for device parameters are shown in brackets. Electrode properties are the mean (max/min) of three values.

Anode	Electrode average transmittance 350–700 nm (%)	Electrode sheet resistance (Ω/\square)	FF (%)	V_{OC} (V)	J_{SC} (mA/cm ²)	PCE (%)
MoO ₃ /Ag/MoO ₃ (60 nm active)	71.7(71.4/72.0)	8.3(8.2/8.5)	60.7 (1.1)	0.801 (0.006)	8.11(0.14)	3.94 (0.12)
TeO ₂ /Ag/MoO ₃ (60 nm active)	77.1(76.9/77.4)	13.9(13.7/14.0)	60.5 (1.0)	0.802 (0.007)	8.70(0.12)	4.22 (0.08)
ITO/MoO ₃ (60 nm active)	83.8(83.6/83.9)	15.9(15.8/16.1)	59.6 (0.7)	0.882 (0.003)	8.54(0.23)	4.49 (0.16)
ITO/MoO ₃ (75 nm active)	83.8 (83.6/83.9)	15.9(15.8/16.1)	59.7 (0.7)	0.885 (0.003)	9.12(0.24)	4.81 (0.09)

worth noting that ITO/MoO₃ devices having an active layer thickness identical to that used in the TAM and MAM devices had a slightly lower PCE of 4.49%, with a comparable yet slightly lower J_{SC} than the TAM devices (8.54 ± 0.23) mA/cm² Current-density against voltage curves for typical solar cells incorporating each different anode are shown in Fig. 5.

It is apparent that the ITO/MoO₃ based devices were also characterised by a larger V_{OC} than were the devices utilising a MAM or TAM anode. This effect has been observed previously in MAM based devices [46,47] and has been attributed to diffusion of Ag through the charge extracting metal oxide layer, although such reductions in V_{OC} are not always observed. It is not clear why such reductions in V_{OC} are not uniformly reported; it is possible that, for example, variations in substrate temperature during the evaporation could result in differences in Ag diffusion. We note, however, that if such a reduction in V_{OC} could be eliminated, then devices utilising the TAM electrode would outperform those based on ITO in which a comparable thickness of active layer has been used.

4. Conclusion

In conclusion, we have fabricated TeO₂/Ag/MoO₃ (TAM) multilayer electrodes that have an average transmittance of 77.1% over the wavelength range of 350–700 nm. This transmittance is larger than the widely investigated multilayer system consisting of MoO₃/Ag/MoO₃ (MAM) that has an average transmittance of only 71.7% over the same wavelength range. When used as the semi-transparent electrode in a polymer solar cell, the improved transmittance of the TAM electrode results in an increased J_{SC} in comparison to devices based on the MAM electrode (8.70 vs 8.11 mA/cm²), leading to a small improvement in power conversion efficiency (4.22 vs 3.94%). We note however that such efficiencies are generally smaller than that of devices based on a conventional ITO electrode that reach an optimised efficiency of 4.81%. We conclude therefore that a TAM multilayer electrode appears to be a promising candidate as an indium free electrode for polymer solar cells, and that tellurium dioxide acts as an efficient seed layer in a multilayer electrode as it encourages the growth of a smooth and continuous silver film.

Acknowledgements

AB acknowledges the EPSRC for funding via the E-Futures Doctoral Training Centre in Interdisciplinary Energy Research EP/G037477/1. We also acknowledge the UK EPSRC for supporting this research through grants EP/J017361/1 (Supersolar Solar Energy Hub) and EP/I028641/1 (Polymer / fullerene photovoltaic devices: new materials and innovative processes for high volume manufacture).

Appendix A. Supplementary material

Supplementary data associated with this article can be found in the online version at <http://dx.doi.org/10.1016/j.solmat.2015.10.010>.

References

- [1] British Petroleum, BP Statistical Review of World Energy, 2015, (www.bp.com/statisticalreview).
- [2] J. Nelson, C.J.M. Emmott, Can solar power deliver? *Phil. Trans. R. Soc. A* **371** (2013) 20120372.
- [3] T. Wang, N.W. Scarratt, H. Yi, A.D.F. Dunbar, A.J. Pearson, D.C. Watters, et al., Fabricating high performance, donor-acceptor copolymer solar cells by spray-coating in air. *Adv. Energy Mater.* **3** (2013) 505–512, <http://dx.doi.org/10.1002/aenm.201200713>.
- [4] R.R. Søndergaard, M. Hösel, F.C. Krebs, Roll-to-roll fabrication of large area functional organic materials. *J. Polym. Sci. Part B Polym. Phys.* **51** (2013) 16–34, <http://dx.doi.org/10.1002/polb.23192>.
- [5] Y. Galagan, I.G. de Vries, A.P. Langen, R. Andriessen, W.J.H. Verhees, S. C. Veenstra, et al., Technology development for roll-to-roll production of organic photovoltaics. *Chem. Eng. Process. Process Intensif.* **50** (2011) 454–461, <http://dx.doi.org/10.1016/j.ccep.2010.07.012>.
- [6] M. Kaltenbrunner, M.S. White, E.D. Glowacki, T. Sekitani, T. Someya, N. S. Sariciftci, et al., Ultrathin and lightweight organic solar cells with high flexibility. *Nat. Commun.* **3** (2012) 770, <http://dx.doi.org/10.1038/ncomms1772>.
- [7] F.C. Krebs, M. Jørgensen, K. Norrman, O. Hagemann, J. Alstrup, T.D. Nielsen, et al., A complete process for production of flexible large area polymer solar cells entirely using screen printing – first public demonstration. *Sol. Energy Mater. Sol. Cells* **93** (2009) 422–441, <http://dx.doi.org/10.1016/j.solmat.2008.12.001>.
- [8] Y. Galagan, D.J.D. Moet, D.C. Hermes, P.W.M. Blom, R. Andriessen, Large area ITO-free organic solar cells on steel substrate. *Org. Electron.* **13** (2012) 3310–3314, <http://dx.doi.org/10.1016/j.orgel.2012.09.039>.
- [9] F.-C. Chen, J.-L. Wu, W.-C. Huang, H.-M.P. Chen, W.-C. Chen, Flexible polymer photovoltaic devices prepared with inverted structures on metal foils. *IEEE Electron Device Lett.* **30** (2009) 727–729, <http://dx.doi.org/10.1109/LED.2009.2022345>.
- [10] A.C. Tolcin, U.S. Geological Survey, 2010, Minerals Yearbook, Indium, n.d.
- [11] N. Espinosa, R. García-Valverde, A. Urbina, F.C. Krebs, A life cycle analysis of polymer solar cell modules prepared using roll-to-roll methods under ambient conditions. *Sol. Energy Mater. Sol. Cells* **95** (2011) 1293–1302, <http://dx.doi.org/10.1016/j.solmat.2010.08.020>.
- [12] A.L. Roes, E.A. Alsema, K. Blok, M.K. Patel, Ex-ante environmental and economic evaluation of polymer photovoltaics. *Prog. Photovolt. Res. Appl.* **17** (2009) 372–393, <http://dx.doi.org/10.1002/pip>.
- [13] R. Paetzold, K. Heuser, D. Henseler, S. Roeger, G. Wittmann, A. Winnacker, Performance of flexible polymeric light-emitting diodes under bending conditions. *Appl. Phys. Lett.* **82** (2003) 3342, <http://dx.doi.org/10.1063/1.1574400>.
- [14] D.R. Cairns, R.P. Witte, D.K. Sparacin, S.M. Sachsman, D.C. Paine, G.P. Crawford, et al., Strain-dependent electrical resistance of tin-doped indium oxide on polymer substrates. *Appl. Phys. Lett.* **76** (2000) 1425, <http://dx.doi.org/10.1063/1.126052>.
- [15] E. Terzini, G. Nobile, T. Polichetti, P. Thilakan, Development and application of low temperature RF magnetron sputtered ITO thin films for a-Si:H based p/i/n junction solar cells, in: Proceedings of the 26th IEEE Photovoltaics Specialist Conference, 1997, pp. 667–670.
- [16] J.A. Thornton, High rate thick film growth. *Annual Rev. Mater. Sci.* **7** (1977) 239–260.
- [17] R. Bel Hadj Tahar, T. Ban, Y. Ohya, Y. Takahashi, Tin doped indium oxide thin films: electrical properties. *J. Appl. Phys.* **83** (1998) 2631, <http://dx.doi.org/10.1063/1.367025>.
- [18] W. Zhang, High-efficiency ITO-free polymer solar cells using highly conductive PEDOT: PSS/surfactant bilayer transparent anodes. *Energy Environ. Sci.* **6** (2013) 1956–1964, <http://dx.doi.org/10.1039/b000000x>.
- [19] Y. Galagan, B. Zimmermann, E.W.C. Coenen, M. Jørgensen, D.M. Tanenbaum, F. C. Krebs, et al., Current collecting grids for ITO-free solar cells. *Adv. Energy Mater.* **2** (2012) 103–110, <http://dx.doi.org/10.1002/aenm.201100552>.
- [20] S.-I. Na, J.-S. Lee, Y.-J. Noh, T.-W. Kim, S.-S. Kim, H.-I. Joh, et al., Efficient ITO-free polymer solar cells with pitch-converted carbon nanosheets as novel solution-processable transparent electrodes. *Sol. Energy Mater. Sol. Cells* **115** (2013) 1–6, <http://dx.doi.org/10.1016/j.solmat.2013.03.019>.
- [21] J.-W. Lim, D.-Y. Cho, S.-I. Na, H.-K. Kim, Simple brush-painting of flexible and transparent Ag nanowire network electrodes as an alternative ITO anode for cost-efficient flexible organic solar cells. *Sol. Energy Mater. Sol. Cells* **107** (2012) 348–354, <http://dx.doi.org/10.1016/j.solmat.2012.07.012>.

- [22] K.-H. Choi, J. Kim, Y.-J. Noh, S.-I. Na, H.-K. Kim, Ag nanowire-embedded ITO films as a near-infrared transparent and flexible anode for flexible organic solar cells, *Sol. Energy Mater. Sol. Cells* 110 (2013) 147–153, <http://dx.doi.org/10.1016/j.solmat.2012.12.022>.
- [23] J.-H. Lee, H.-S. Shin, Y.-J. Noh, S.-I. Na, H.-K. Kim, Brush painting of transparent PEDOT/Ag nanowire/PEDOT multilayer electrodes for flexible organic solar cells, *Sol. Energy Mater. Sol. Cells* 114 (2013) 15–23, <http://dx.doi.org/10.1016/j.solmat.2013.02.020>.
- [24] V. Shrotriya, G. Li, Y. Yao, C.-W. Chu, Y. Yang, Transition metal oxides as the buffer layer for polymer photovoltaic cells, *Appl. Phys. Lett.* 88 (2006) 073508, <http://dx.doi.org/10.1063/1.2174093>.
- [25] R. Steim, F.R. Kogler, C.J. Brabec, Interface materials for organic solar cells, *J. Mater. Chem.* 20 (2010) 2499–2512, <http://dx.doi.org/10.1039/b921624c>.
- [26] J.C.C. Fan, Transparent heat-mirror films of $\text{TiO}_2/\text{Ag}/\text{TiO}_2$ for solar energy collection and radiation insulation, *Appl. Phys. Lett.* 25 (1974) 693, <http://dx.doi.org/10.1063/1.1655364>.
- [27] C. Guillén, J. Herrero, TCO/metal/TCO structures for energy and flexible electronics, *Thin Solid Films* 520 (2011) 1–17, <http://dx.doi.org/10.1016/j.tsf.2011.06.091>.
- [28] H. Lei, P. Qin, W. Ke, Y. Guo, X. Dai, Z. Chen, et al., Performance enhancement of polymer solar cells with high work function CuS modified ITO as anodes, *Org. Electron.* 22 (2015) 173–179, <http://dx.doi.org/10.1016/j.orgel.2015.03.051>.
- [29] F. Cheng, G. Fang, X. Fan, H. Huang, Q. Zheng, P. Qin, et al., Enhancing the performance of P3HT:ICBA based polymer solar cells using LiF as electron collecting buffer layer and UV-ozone treated MoO_3 as hole collecting buffer layer, *Sol. Energy Mater. Sol. Cells* 110 (2013) 63–68, <http://dx.doi.org/10.1016/j.solmat.2012.12.006>.
- [30] F. Li, S. Ruan, Y. Xu, F. Meng, J. Wang, W. Chen, et al., Semitransparent inverted polymer solar cells using $\text{MoO}_3/\text{Ag}/\text{WO}_3$ as highly transparent anodes, *Sol. Energy Mater. Sol. Cells* 95 (2011) 877–880, <http://dx.doi.org/10.1016/j.solmat.2010.11.009>.
- [31] D.-T. Nguyen, S. Vedraïne, L. Cattin, P. Torchio, M. Morsli, F. Flory, et al., Effect of the thickness of the MoO_3 layers on optical properties of $\text{MoO}_3/\text{Ag}/\text{MoO}_3$ multilayer structures, *J. Appl. Phys.* 112 (2012) 063505, <http://dx.doi.org/10.1063/1.4751334>.
- [32] L. Cattin, M. Morsli, F. Dahou, S.Y. Abe, A. Khelil, J.C. Bernède, Investigation of low resistance transparent $\text{MoO}_3/\text{Ag}/\text{MoO}_3$ multilayer and application as anode in organic solar cells, *Thin Solid Films* 518 (2010) 4560–4563, <http://dx.doi.org/10.1016/j.tsf.2009.12.031>.
- [33] N.P. Sergeant, A. Hadipour, B. Niesen, D. Cheyns, P. Heremans, P. Peumans, et al., Design of transparent anodes for resonant cavity enhanced light harvesting in organic solar cells, *Adv. Mater.* 24 (2012) 728–732, <http://dx.doi.org/10.1002/adma.201104273>.
- [34] J.-F. Salinas, H.-L. Yip, C.-C. Chueh, C.-Z. Li, J.-L. Maldonado, A.K.-Y. Jen, Optical design of transparent thin metal electrodes to enhance in-coupling and trapping of light in flexible polymer solar cells, *Adv. Mater.* 24 (2012) 6362–6367, <http://dx.doi.org/10.1002/adma.201203099>.
- [35] G.F. Burkhard, E.T. Hoke, M.D. McGehee, Accounting for interference, scattering, and electrode absorption to make accurate internal quantum efficiency measurements in organic and other thin solar cells, *Adv. Mater.* 22 (2010) 3293–3297, <http://dx.doi.org/10.1002/adma.201000883>.
- [36] F. Li, Z. Lin, B. Zhang, Y. Zhang, C. Wu, T. Guo, Fabrication of flexible conductive graphene/Ag/Al-doped zinc oxide multilayer films for application in flexible organic light-emitting diodes, *Org. Electron.* 14 (2013) 2139–2143, <http://dx.doi.org/10.1016/j.orgel.2013.05.023>.
- [37] F. Nehm, S. Schubert, L. Müller-Meskamp, K. Leo, Observation of feature ripening inversion effect at the percolation threshold for the growth of thin silver films, *Thin Solid Films* 556 (2014) 381–384, <http://dx.doi.org/10.1016/j.tsf.2014.01.067>.
- [38] H.-K. Park, J.-W. Kang, S.-I. Na, D.-Y. Kim, H.-K. Kim, Characteristics of indium-free GZO/Ag/GZO and AZO/Ag/AZO multilayer electrode grown by dual target DC sputtering at room temperature for low-cost organic photovoltaics, *Sol. Energy Mater. Sol. Cells* 93 (2009) 1994–2002, <http://dx.doi.org/10.1016/j.solmat.2009.07.016>.
- [39] I.P. Lopéz, L. Cattin, D.-T. Nguyen, M. Morsli, J.C. Bernède, Dielectric/metal/dielectric structures using copper as metal and MoO_3 as dielectric for use as transparent electrode, *Thin Solid Films* 520 (2012) 6419–6423, <http://dx.doi.org/10.1016/j.tsf.2012.06.056>.
- [40] D. Zhang, H. Yabe, E. Akita, P. Wang, R. Murakami, X. Song, Effect of silver evolution on conductivity and transmittance of ZnO/Ag thin films, *J. Appl. Phys.* 109 (2011) 104318, <http://dx.doi.org/10.1063/1.3592975>.
- [41] K.-H. Choi, H.-J. Nam, J.-A. Jeong, S.-W. Cho, H.-K. Kim, J.-W. Kang, et al., Highly flexible and transparent $\text{InZnSnO}_x/\text{Ag}/\text{InZnSnO}_x$ multilayer electrode for flexible organic light emitting diodes, *Appl. Phys. Lett.* 92 (2008) 223302, <http://dx.doi.org/10.1063/1.2937845>.
- [42] W.-F. Xu, C.-C. Chin, D.-W. Hung, P.-K. Wei, Transparent electrode for organic solar cells using multilayer structures with nanoporous silver film, *Sol. Energy Mater. Sol. Cells* 118 (2013) 81–89, <http://dx.doi.org/10.1016/j.solmat.2013.07.047>.
- [43] D. Jeannot, J. Pinard, P. Ramoni, E.M. Jost, Physical and chemical properties of metal oxide additions to Ag-SnO_2 contact materials and predictions of electrical performance, *IEEE Trans. Compon. Packag. Manuf. Technol.* 17 (1994) 17–23.
- [44] S. Schubert, J. Meiss, L. Müller-Meskamp, K. Leo, Improvement of transparent metal top electrodes for organic solar cells by introducing a high surface energy seed layer, *Adv. Energy Mater.* 3 (2013) 438–443, <http://dx.doi.org/10.1002/aenm.201200903>.
- [45] Z. Wang, C. Zhang, R. Gao, D. Chen, S. Tang, J. Zhang, et al., Improvement of transparent silver thin film anodes for organic solar cells with a decreased percolation threshold of silver, *Sol. Energy Mater. Sol. Cells* 127 (2014) 193–200, <http://dx.doi.org/10.1016/j.solmat.2014.04.024>.
- [46] L. Cattin, Y. Lare, M. Makha, M. Fleury, F. Chandezon, T. Abachi, et al., Effect of the Ag deposition rate on the properties of conductive transparent $\text{MoO}_3/\text{Ag}/\text{MoO}_3$ multilayers, *Sol. Energy Mater. Sol. Cell.* 117 (2013) 103–109, <http://dx.doi.org/10.1016/j.solmat.2013.05.026>.
- [47] T. Abachi, L. Cattin, G. Louarn, Y. Lare, A. Bou, M. Makha, et al., Highly flexible, conductive and transparent $\text{MoO}_3/\text{Ag}/\text{MoO}_3$ multilayer electrode for organic photovoltaic cells, *Thin Solid Films* 545 (2013) 438–444, <http://dx.doi.org/10.1016/j.tsf.2013.07.048>.